COMMUNICATION

Check for updates

Development of a selective-iodide indicator for live-cell imaging and evaluation of CFTR activity

Jared Morse,†[ab] Prasanna Ganesh,†[a] Kathrine Cowart,[a] Gabriella Ballestas,[ab] Fung Kit Tang[a] and Kaho Leung ID *[abc]

Cystic fibrosis (CF) arises from mutations in the cystic fibrosis transmembrane conductance regulator (CFTR) gene. Monitoring I^- transport serves as a critical approach for evaluating CFTR function in live cells, providing a foundation for the development of diagnostic tools and therapeutic treatments. Here, we report an iridium(III) complex (**I-Sense**) for the selective and pH-independent imaging of intracellular I^-. By tracking cellular iodide I^- uptake, **I-Sense** facilitates the evaluation of CFTR activity in live cells, providing a valuable tool for the functional characterization of CFTR activity.

The cystic fibrosis transmembrane conductance regulator (CFTR) is an ATP-gated anion channel that mediates the transport of chloride and bicarbonate ions.[1] Mutations in the *CFTR* gene cause cystic fibrosis (CF), an autosomal recessive disorder characterized by thickened mucus secretions, chronic infections, and progressive lung disease.[2] To date, over 2000 distinct *CFTR* mutations have been reported.[3] CF compromises CFTR function through diverse molecular mechanisms, including impaired protein misfolding, trafficking, reduced surface stability, and ion conductance.[4–6] The mechanistic heterogeneity reveals the importance for personalized functional assessment of CFTR activity and therapeutic efficacy.[4,7]

In recent years, CFTR modulators such as combination therapies like Trikafta have revolutionized CF treatment.[8–11] These therapies enhance the function of defective CFTR. However, substantial inter-individual variability in therapeutic response is observed among CF patients. Consequently, functional assays that assess CFTR activity in patient-derived cells are essential for guiding personalized therapeutic strategies and enabling treatment access for individuals

carrying rare or uncharacterized CFTR variants.[12–14] Traditional diagnostic approaches such as sweat chloride testing and nasal potential difference measurements, are clinically established but often lack the resolution to assess subtle functional differences or treatment responses at the cellular level.[15] Live-cell imaging has been important in elucidating cell health and processes.[16,17] It was employed to assess CFTR activity based on its ability to mediate the transport of halide ions, such as I^-, which is not endogenously abundant in cells; intracellular I^- concentration is 10 000–100 000 fold less than chloride. This unique ion distribution permits the evaluation of CFTR function.[7,18] Non-selective halide sensors have been used to monitor the CFTR-mediated cellular uptake of I^-, as providing a functional readout of CFTR activity.[18] These include genetically encoded fluorescent proteins, such as YFP-based halide sensors,[19–21] as well as small-molecule indicator MQAE.[22–25] These tools have been instrumental in assessing CFTR activity by monitoring intracellular I^-. However, both sensors exhibit notable limitations as they detect Cl^- which is highly abundant in cells, as it pays a crucial role in cell homeostasis.[26] Furthermore, fluorescent protein-based halide sensors are pH-sensitive, whereby fluctuations in cytosolic pH can confound signal interpretation. In contrast, the small-molecule indicator MQAE enables pH-independent detection of halide ions but it is limited by poor cellular uptake, limited intracellular fluorescence brightness, and high susceptibility to photobleaching.[27] Therefore, there is an urgent need for an imaging tool capable of visualizing intracellular I^- in live cells to evaluate CFTR activity.[27]

Live-cell imaging is a widely utilized approach to directly assess ion transport mediated by ion channels and transporters in cells.[28,29] Cyclometallated iridium(III) complexes have attracted considerable interest as luminescent probes due to their favourable photophysical properties, such as synthetic modularity, large Stokes shifts, and notably long phosphorescent lifetimes.[30–33] These prolonged emission lifetimes enable time-resolved imaging

[a] Department of Chemistry & Biochemistry, Clarkson University, NY 13676, USA
[b] Department of Chemistry & Biochemistry, University of South Carolina, Columbia, SC 29208, USA. E-mail: KAHO@mailbox.sc.edu
[c] South Carolina SmartState Centers for Neurotherapeutics, University of South Carolina, Columbia, SC 29208, USA
† These authors contributed equally.

strategies that effectively reduce background autofluorescence in complex biological systems.[34–36] Their robustness and adaptability place cyclometallated iridium(III) complexes as powerful tools in the development of sensitive indicators for live-cell imaging.[37,38] We herein synthesized and characterized a phosphorescent iridium(III) complex, referred to as **I-Sense**, based on the reported protocol (Fig. 1a and S1–S4).[39,40] **I-Sense** exhibits a broad emission maximum at 530 nm, with a substantial Stokes shift of 180 nm upon excitation at 360 nm. The quantum yield of **I-Sense** decreases significantly upon addition of I^- (Table S1). Fluorescence titration assay revealed that incremental addition of I^- (0–1 mM) resulted in a concentration-dependent decrease in the emission intensity of **I-Sense** at 530 nm (Fig. 1b–d). These results demonstrate the high sensitivity of **I-Sense** toward I^- detection in the micromolar range, in contrast to existing halide indicators for CFTR activity, which typically require millimolar iodide concentrations.[41] The limit of detection for I^- was calculated to be 10.8 μM, this is above the cellular physiological range and indicates **I-Sense** only monitors our induced cellular I^- environments. Furthermore, the selectivity of **I-Sense** for I^- was examined by comparing fluorescence responses in the presence of a panel of physiologically relevant anions or reactive oxygen species (Fig. 1e and S5).[42] **I-Sense** exhibited significant fluorescence quenching exclusively in the presence of I^-. Thus, indicating it's high selectivity toward I^- detection.

Next, we examined the pH-sensitivity of **I-Sense**. The emission intensity ratio (I_0/I_F) increases steadily with increasing [I^-], and minimal variation in fold change and detection sensitivity across a range of physiological pH values, indicating that it's I^--sensing capability is pH-independent (Fig. 2a). This trend in detection is shown in a 3D surface plot (Fig. 2b). A linearly proportional normalized
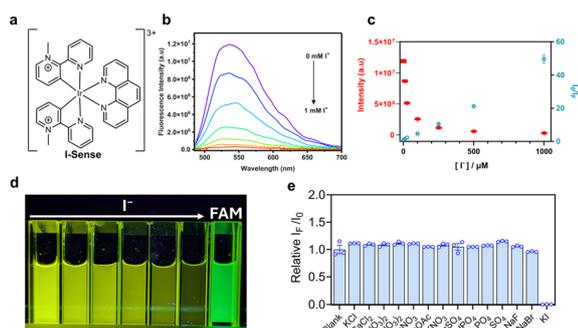

Fig. 2 **I-Sense** selectively detects I^- in a pH-independent manner. (a) Stern–Volmer plot of **I-Sense** (10 μM) with increasing [I^-] in different pH values upon excitation at 360 nm. Normalized emission intensity ratio (I_0/I_F) of **I-Sense** represented as a function of [I^-] at pH 4.5, 4.8, 5.0, 5.5, 6.0, 6.5, and 7.0. Values were normalized to I_0/I_F at [I^-] at 0 mM. (b) Calibration surface plot of I_0/I_F of **I-Sense** as a function of [I^-] and pH measured in 5 mM sodium phosphate buffer (150 mM KNO_3, 5 mM $NaNO_3$, 1 mM $Ca(NO_3)_2$, and 1 mM $Mg(NO_3)_2$). (c) Normalized fluorescence intensity ratio (I_0/I_F) of **I-Sense** in the presence of 0 μM, 10 μM, 100 μM, 250 μM, 500 μM, and 1000 μM I^- in sodium phosphate buffer at indicated pH. (d) Phosphorescence lifetime decay curve of **I-Sense** with 0 mM (black), 0.5 mM (green) and 1 mM (yellow) I^- in 5 mM phosphate buffer at pH 7.0. (e) Phosphorescence lifetime values of **I-Sense** derived from lifetime decay plot (d). (f) Stern–Volmer plot of **I-Sense** for I^- detection in physiological ionic environment. $X_0/X_F = I_0/I_F$ (intensity) or T_0/T_F (lifetime), values were normalized to X_0/X_F at [I^-] = 0 mM. Error bars indicate the mean ± standard error of the mean (s.e.m.) of three independent measurements.

Fig. 1 **I-Sense** selectively detects I^- in vitro. (a) Chemical structure of **I-Sense**. (b) Emission spectrum of **I-Sense** in the presence of 0–1 mM I^- upon excitation at 360 nm. (c) Luminescence intensity at 530 nm (red) and Stern–Volmer plot (blue) of **I-Sense** (10 μM) with increasing [I^-] in sodium phosphate buffer (5 mM, pH 7.2) upon excitation at 360 nm. (d) Photo of **I-Sense** with increasing concentration of I^- and 5 μM fluorescein under UV illumination. (e) Luminescence response of **I-Sense** given by the fold change of I_F/I_0 in the presence of different physiological ions (100 mM). Error bars indicate the mean ± standard error of the mean (s.e.m.) of three independent measurements.

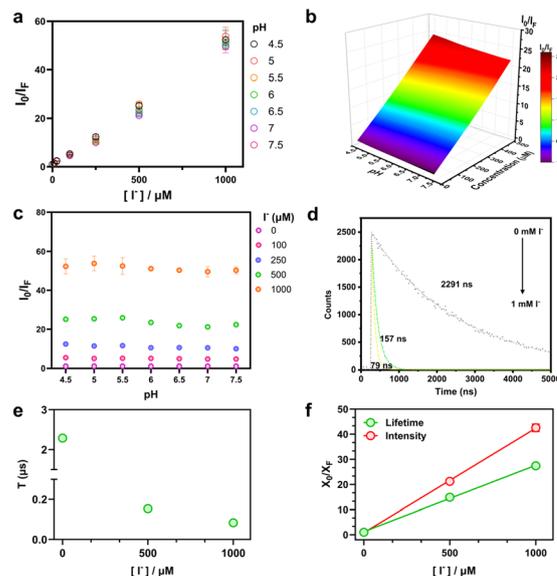emission intensity ratio (I_0/I_F) to [I^-] independent of pH can be seen. In Fig. 2c, we also see the consistent fold change of I_0/I_F across 0 to 1000 μM I^- while staying uniform across the pH range of 4.5 to 7.5, confirming unaffected I^--sensing in different pH. Additionally, phosphorescence lifetime decay of **I-Sense** was measured in the presence of I^- under air-equilibrated aqueous conditions. Upon incremental addition of I^- a marked quenching of the phosphorescence lifetime was observed, decreasing from 2.29 μs to 79 ns (Fig. 2d–f). Both the Stern–Volmer plot of lifetime decay values and emission intensity (Fig. 2f) shows a linear correlation with [I^-] upon addition of iodide, consistent with dynamic quenching behavior.

I-Sense was evaluated as an imaging probe for intracellular I^-. It's cytotoxicity profile was assessed, revealing minimal toxicity under the tested conditions. This supports the biocompatibility of **I-Sense** and its suitability for live-cell imaging applications (Fig. S6). Next, we evaluated **I-Sense**'s ability to sense intracellular I^- following its success with in vitro testing under physiological conditions. The positive charge of **I-Sense**

confers high water solubility and facilitates efficient cellular uptake in the absence of any pretreatment. Upon pulse and chase, **I-Sense** efficiently distributes throughout the cytosol in all three tested cell types, indicating its broad cell permeability and versatility across diverse cellular contexts (Fig. 3a, c and e).

As shown in Fig. 3a–f, **I-Sense**-labeled-cells demonstrated substantially higher whole-cell phosphorescence intensity compared with the autofluorescence, while the intensity of the **I-Sense**-labeled-cells was lowered by 50% upon treatment of I⁻. To further evaluate **I-Sense's** sensitivity to intracellular I⁻, in-cell I⁻ calibration was performed using established protocols; cells were treated with varying concentrations of iodide.[23,43] **I-Sense**-labeled-cells showed a concentration-dependent decrease in whole-cell fluorescence intensity upon increasing [I⁻] (Fig. 3g and h). The results of

the in-cell I⁻ calibration align with the *in vitro* calibration, supporting the reliability of intracellular I⁻ quantification of **I-Sense**.

Given the ability of **I-Sense** to monitor intracellular I⁻, we next investigated its capability in assessing I⁻ uptake as a functional indicator of CFTR channel activity. Using primary skin fibroblasts derived from patients with cystic fibrosis, we examined both impaired I⁻ transport due to defective CFTR and, the pharmacological rescue of CFTR function upon treatment with an activator. Ivacaftor was used to enhance CFTR activity by promoting gating function, particularly in CFTR variants that exhibit impaired conductance.[8,10,44] Fluorescence signal in untreated patient fibroblasts (Fig. 4a) revealed minimal signal quenching following I⁻ stimulation in CF patients compared to the normal individual (NI). This indicates impaired anion permeability in the CF patient cells.
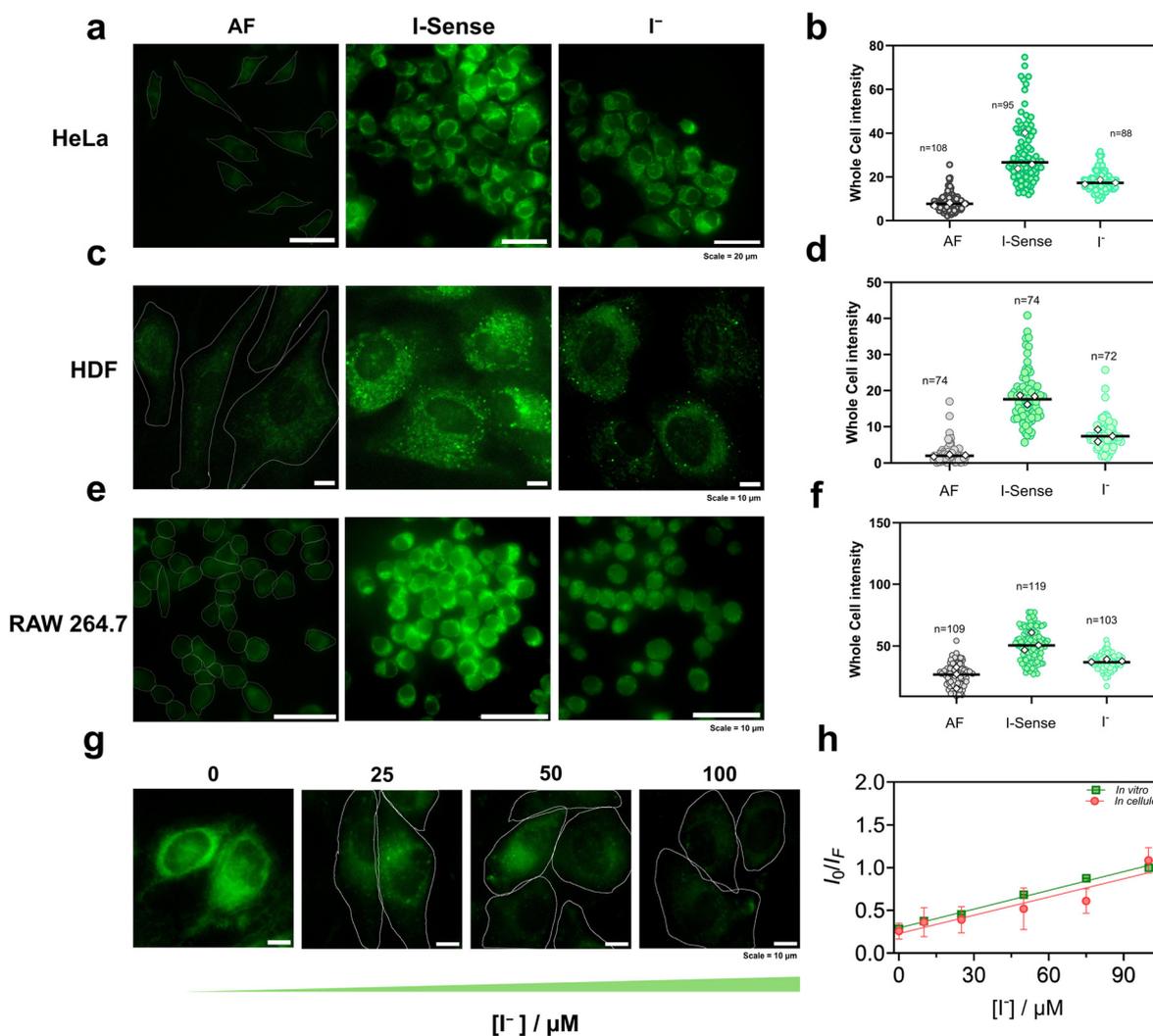

Fig. 3 **I-Sense** detects intracellular I⁻. (a, c and e) Representative fluorescence images of **I-Sense**-labelled (a) HeLa (c) HDF and (e) RAW 264.7 cells, with and without incubation of 75 mM I⁻. AF indicates autofluorescence. (b, d and f) Scatter plot of the whole cell intensities quantification of (a), (c) and (e). (g) Representative fluorescence images of **I-Sense**-labeled HDF cells clamped in various [I⁻]. (h) *In vitro* (green) and *in cellulo* (red) I⁻ calibration of **I-Sense**. Experiments were performed in triplicate. The median of all trials is given by a line. The median value of individual trial is given by a diamond symbol (*n* = number of cells). Error bars indicate the mean ± standard error of the mean (s.e.m.) of three independent measurements.
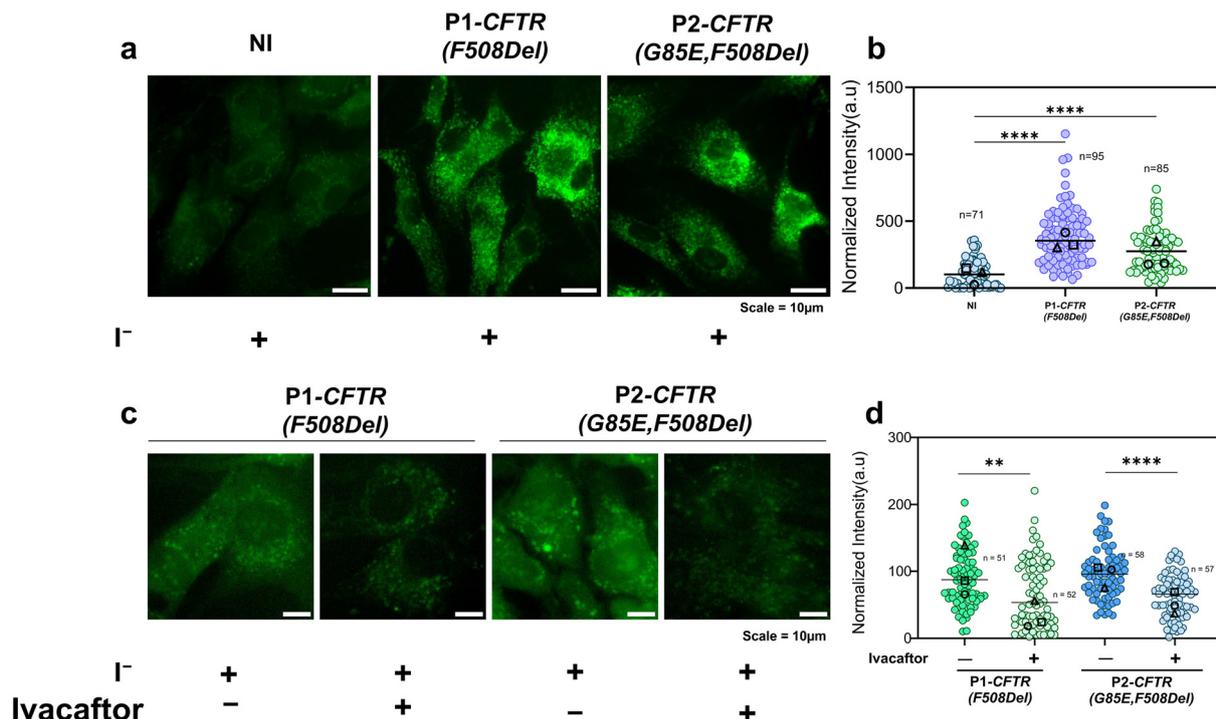
Fig. 4 **I-Sense** functions as a molecular reporter for CFTR activity by quantifying cellular I⁻ uptake in cells derived from cystic fibrosis patients. (a) Representative fluorescence images of **I-Sense**-labeled primary skin fibroblasts from apparently healthy normal individuals and CFTR patients with identified mutations (F508Del, G85E) after 500 μM I⁻ stimulation. (b) Quantification of whole cell intensity of (a). (c) Representative fluorescence images of **I-Sense**-labeled CFTR patient fibroblasts treated with and without 2 μM ivacaftor after 500 μM I⁻ stimulation. (d) Quantification of whole cell intensity of (c). Experiments were performed in triplicate for each cell line. The median value of each trial is given by square, circle, and triangle symbols. One-way analysis of variance (ANOVA) followed by Dunnett's test for multiple comparison. **$P < 0.01$; ****$P < 0.0001$.

Quantification (Fig. 4b) of fluorescence intensity of **I-Sense**-labeled cells shows the significantly reduced I⁻-mediated quenching in CF samples compared to NI. Upon treatment with ivacaftor, a notable increase in fluorescence quenching was observed. This indicates enhanced cellular uptake of I⁻. This effect may be attributed to the pharmacological rescue of CFTR activity. Quantitative analysis of whole-cell fluorescence intensity further validated this response, revealing a statistically significant increase in I⁻ uptake following ivacaftor administration. These results suggest that **I-Sense** holds potential as a tool for distinguishing I⁻ uptake differences between healthy individuals and CF patients. Moreover, it may serve as a useful tool for monitoring the therapeutic efficacy of candidate CF treatments.

The development of the phosphorescent cyclometallated iridium(III) complex **I-Sense** represents a notable advancement in the imaging toolbox for probing CFTR function. Existing halide-sensitive indicators typically respond to a broad spectrum of halides, including Cl⁻, Br⁻, and I⁻, few enable selective and pH-independent I⁻ detection. In contrast, **I-Sense** displays marked selectivity toward I⁻, exhibiting high sensitivity and minimal response by other physiological anions such as Cl⁻ and Br⁻, thereby offering a robust approach for I⁻ imaging in live cells. In conclusion, we synthesized and characterized a phosphorescent iridium(III) complex **I-Sense**, capable of highly sensitive,

selective, and pH-independent detection of I⁻. A notable advantage of **I-Sense** lies in its extended phosphorescence lifetime, enabling reliable detection and monitoring of I⁻. Furthermore, its dual-mode response, exhibiting both intensity- and lifetime-based detection of I⁻, provides a robust and versatile platform for evaluating CFTR activation. It permits sensitive detection of I⁻ in the micromolar range and reveals the differences in I⁻ uptake between primary fibroblasts derived from healthy individuals and those from cystic fibrosis patients. These features position **I-Sense** as a powerful tool with strong potential for fundamental research, drug screening, and potentially evaluation of CFTR modulators.

Author contributions

Jared Morse: writing – original draft, writing – review & editing, visualization, validation, software, methodology, investigation, formal analysis, data curation, supervision, project administration, conceptualization. Prasanna Ganesh: writing – original draft, visualization, software, methodology, investigation, formal analysis, data curation. Kathrine Cowart: investigation, formal analysis, data curation. Gabriella Ballestas: writing – original draft, writing – review & editing, visualization, validation, software, investigation, formal analysis. Fung Kit Tang: data curation, visualization,

Conflicts of interest

There are no conflicts to declare.

Data availability

Supplementary information: Experimental protocols, synthetic information and supplemental data are provided in the SI. See DOI: **https://doi.org/10.1039/D5SD00086F**.

Data are available from the corresponding author upon reasonable request.

Acknowledgements

Notes and references

1 M. A. Mall, P.-R. Burgel, C. Castellani, J. C. Davies, M. Salathe and J. L. Taylor-Cousar, *Nat. Rev. Dis. Primers*, 2024, **10**, 53.

2 H. Grasemann and F. Ratjen, *N. Engl. J. Med.*, 2023, **389**, 1693–1707.

3 N. Sharma and G. R. Cutting, *J. Cystic Fibrosis*, 2020, **19**(Suppl 1), S5–S9.

4 M. M. Ensinck, L. De Keersmaecker, A. S. Ramalho, S. Cuyx, S. Van Biervliet, L. Dupont, F. Christ, Z. Debyser, F. Vermeulen and M. S. Carlon, *ERJ Open Res.*, 2022, **8**(2), DOI: **10.1183/23120541.00716-2021**.

5 L. S. Ostedgaard, D. K. Meyerholz, J.-H. Chen, A. A. Pezzulo, P. H. Karp, T. Rokhlina, S. E. Ernst, R. A. Hanfland, L. R. Reznikov, P. S. Ludwig, M. P. Rogan, G. J. Davis, C. L. Dohrn, C. Wohlford-Lenane, P. J. Taft, M. V. Rector, E. Hornick, B. S. Nassar, M. Samuel, Y. Zhang, S. S. Richter, A. Uc, J. Shilyansky, R. S. Prather, P. B. McCray, J. Zabner, M. J. Welsh and D. A. Stoltz, *Sci. Transl. Med.*, 2011, **3**, 74ra24.

6 *Cystic Fibrosis*, ed. M. D. Amaral and K. Kunzelmann, Humana Press, Totowa, NJ, 2011, vol. 741.

7 A. S. Ramalho, M. Boon, M. Proesmans, F. Vermeulen, M. S. Carlon and K. D. Boeck, *Int. J. Mol. Sci.*, 2022, **23**(3), DOI: **10.3390/ijms23031437**.

8 H. Yu, B. Burton, C.-J. Huang, J. Worley, D. Cao, J. P. Johnson, A. Urrutia, J. Joubran, S. Seepersaud, K. Sussky, B. J. Hoffman and F. Van Goor, *J. Cystic Fibrosis*, 2012, **11**, 237–245.

9 S. H. Donaldson, J. M. Pilewski, M. Griese, J. Cooke, L. Viswanathan, E. Tullis, J. C. Davies, J. A. Lekstrom-Himes, L. T. Wang and VX11-661-101 Study Groups, *Am. J. Respir. Crit. Care Med.*, 2018, **197**, 214–224.

10 I. Sermet-Gaudelus, *Eur. Respir. Rev.*, 2013, **22**, 66–71.

11 *Elexacaftor-Tezacaftor-Ivacaftor and Ivacaftor (Trikafta): CADTH Reimbursement Review: Therapeutic area: Cystic fibrosis, F508del-CFTR mutation, 6 years and older*, Canadian Agency for Drugs and Technologies in Health, Ottawa (ON), 2022.

12 S. Y. Graeber, A. Balázs, N. Ziegahn, T. Rubil, C. Vitzthum, L. Piehler, M. Drescher, K. Seidel, A. Rohrbach, J. Röhmel, S. Thee, J. Duerr, M. A. Mall and M. Stahl, *Int. J. Mol. Sci.*, 2023, **24**(15), DOI: **10.3390/ijms241512365**.

13 Z. Cai, J. Liu, H. Li and D. N. Sheppard, *Acta Pharmacol. Sin.*, 2011, **32**, 693–701.

14 M. W. Wooten, V. L. Rudick, M. J. Rudick and M. L. Higgins, *In Vitro Cell. Dev. Biol.*, 1985, **21**, 207–215.

15 D.-T. Anton-Păduraru, A. N. Azoicăi, F. Trofin, D. E. Mîndru, A. M. Murgu, A. S. Bocec, C. O. Iliescu Haliţchi, C. I. Ciongradi, I. Sârbu and M. L. Iliescu, *Diagnostics*, 2024, **14**(7), DOI: **10.3390/diagnostics14070763**.

16 J. Morse and K. H. Leung, *Sens. Actuators Rep.*, 2025, **9**, 100259.

17 F. K. Tang, L. Tucker, M. R. Nadiveedhi, C. Hladun, J. Morse, M. Ali, N. Payne, M. Schmidt and K. Leung, *BioRxiv*, 2024, preprint, DOI: **10.1101/2024.08.22.609247**.

18 L. V. Galietta, S. Jayaraman and A. S. Verkman, *Am. J. Physiol.*, 2001, **281**, C1734–C1742.

19 L. J. Galietta, P. M. Haggie and A. S. Verkman, *FEBS Lett.*, 2001, **499**, 220–224.

20 B. C. Campbell, M. G. Paez-Segala, L. L. Looger, G. A. Petsko and C. F. Liu, *Nat. Methods*, 2022, **19**, 1612–1621.

21 W. Peng, C. C. Maydew, H. Kam, J. K. Lynd, J. N. Tutol, S. M. Phelps, S. Abeyrathna, G. Meloni and S. C. Dodani, *Chem. Sci.*, 2022, **13**, 12659–12672.

22 J. Biwersi and A. S. Verkman, *Biochemistry*, 1991, **30**, 7879–7883.

23 J. Morse, N. Ofodum, F. K. Tang, M. Schmidt, X. Lu and K. Leung, *ACS Sens.*, 2025, **10**, 657–663.

24 J. Morse, M. R. Nadiveedhi, M. Schmidt, F.-K. Tang, C. Hladun, P. Ganesh, Z. Qiu and K. Leung, *BioRxiv*, 2024, preprint, DOI: **10.1101/2024.08.08.606814**.

25 A. S. Verkman, M. C. Sellers, A. C. Chao, T. Leung and R. Ketcham, *Anal. Biochem.*, 1989, **178**, 355–361.

26 J. Morse, D. Wang, S. Mei, D. Whitham, C. Hladun, C. C. Darie, H. O. Sintim, M. Wang and K. Leung, *BioRxiv*, 2024, preprint, DOI: **10.1101/2024.04.08.588475**.

27 L. A. W. Vijftigschild, C. K. van der Ent and J. M. Beekman, *Cytometry, Part A*, 2013, **83**, 576–584.

28 J. Osei-Owusu, Z. Ruan, L. Mihaljević, D. S. Matasic, K. H. Chen, W. Lü and Z. Qiu, *eLife*, 2022, **11**, DOI: **10.7554/eLife.82955**.

29 J. Osei-Owusu, J. Yang, K. H. Leung, Z. Ruan, W. Lü, Y. Krishnan and Z. Qiu, *Cell Rep.*, 2021, **34**, 108683.

30 S. Ilic, D. R. Cairnie, C. M. Bridgewater and A. J. Morris, *J. Photochem. Photobiol.*, 2021, **8**, 100084.

31 D.-L. Ma, H.-Z. He, K.-H. Leung, D. S.-H. Chan and C.-H. Leung, *Angew. Chem., Int. Ed.*, 2013, **52**, 7666–7682.

32 Z. Ruan, J. Yang, Y. Li and K. Y. Zhang, *ChemBioChem*, 2024, **25**, e202400094.

33 J. Zhou, J. Li, K. Y. Zhang, S. Liu and Q. Zhao, *Coord. Chem. Rev.*, 2022, **453**, 214334.

34 G. Marriott, R. M. Clegg, D. J. Arndt-Jovin and T. M. Jovin, *Biophys. J.*, 1991, **60**, 1374–1387.

35 M. Y. Berezin and S. Achilefu, *Chem. Rev.*, 2010, **110**, 2641–2684.

36 Y. You, S. Cho and W. Nam, *Inorg. Chem.*, 2014, **53**, 1804–1815.

37 S. Kuang, F. Wei, J. Karges, L. Ke, K. Xiong, X. Liao, G. Gasser, L. Ji and H. Chao, *J. Am. Chem. Soc.*, 2022, **144**, 4091–4101.

38 C. Jin, J. Liu, Y. Chen, R. Guan, C. Ouyang, Y. Zhu, L. Ji and H. Chao, *Sci. Rep.*, 2016, **6**, 22039.

39 K. Laws, A. Eskandari, C. Lu and K. Suntharalingam, *Chem. – Eur. J.*, 2018, **24**, 15205–15210.

40 A. Kamecka, O. Grochowska and A. Kapturkiewicz, *Inorg. Chem. Commun.*, 2019, **108**, 107547.

41 S. Jayaraman and A. S. Verkman, *Biophys. Chem.*, 2000, **85**, 49–57.

42 H. Sies and D. P. Jones, *Nat. Rev. Mol. Cell Biol.*, 2020, **21**, 363–383.

43 S. Saha, V. Prakash, S. Halder, K. Chakraborty and Y. Krishnan, *Nat. Nanotechnol.*, 2015, **10**, 645–651.

44 V. Tomati, V. Capurro, E. Pesce, C. Pastorino, E. Sondo, M. Lena, A. Borrelli, F. Cresta, S. Pantano, F. Collini, P. Ripani, V. Terlizzi, C. Fevola, S. Costa, M. C. Lucanto, F. Zara, T. Bandiera, R. Bocciardi, C. Castellani, L. J. V. Galietta and N. Pedemonte, *Front. Pharmacol.*, 2024, **15**, 1494327.